Journal of Molecular Modeling (2024) 30:100
https://doi.org/10.1007/s00894-024-05898-0

ORIGINAL PAPER

A theoretical study on 1H-indole-2,3-dione complexes with lithium, sodium, and potassium cations

Fatma Genc[1] · Fatma Kandemirli[2] · Serap Senturk Dalgic[3]

Received: 25 October 2023 / Accepted: 4 March 2024 / Published online: 11 March 2024

Abstract

Context A comparative study of the change in different properties of electronic and structural of the free 1H-indole-2,3-dione molecule and its complexes has been obtained. HOMA analysis was performed to investigate the effects of lithium sodium and potassium cations on the aromaticity of lithium sodium and potassium complexes of 1H-indole-2,3-dione.

Methods Several 1H-indole-2,3-dione complexes with lithium, sodium, and potassium cations were optimized at the B3LYP/6-311G(d,p) level. The cation and π interaction has been investigated from different aspects, including interaction energy calculations, charge transfer values, and changes in the aromaticity of the ring upon complexation. The charge transfer and natural population analysis for the complexes were performed with the natural bond orbital (NBO) analysis. The properties of bond critical points in complexes were studied by applying the quantum theory of atoms in molecules (QTAIM). Finally, the aromaticity change of phenyl induced upon complex formation was evaluated by applying the harmonic oscillator model of aromaticity (HOMA). $[Li\text{-}IN_a]^+$ and $[[Li\text{-}IN_b]^+$ were optimized with the wB97XD function using a version of Grimme's D2 dispersion model, and the absorption energy was compared with the calculation made with the B3LYP functional.

Keywords Charge transfer · HOMA · Frontier molecular orbital · Mulliken atomic charges · Quantum theory · Natural bond orbital

Introduction

The biological properties of 1H-indole-2,3-dione, called Isatin IN, involve a wide variety of actions in the brain, protect against certain types of infections [1], and possess central nervous system-monoaminooxidase (CNS-MAO) inhibition, anticonvulsant, and anxiogenic activities [2]. In humans, IN is a metabolic derivative of adrenaline [3]. IN is important in organic chemistry as it can be used to synthesize various heterocyclic compounds such as INs, quinolines, and indoles [4].

With a combination of theoretical calculations and related isodesmic reactions, they stated that IN has some antiaromatic characteristics and isotonic anhydride has some aromatic stabilizations [5]. The encapsulation process of the anticancer drug IN was studied in a capped (10,10) single-walled carbon nanotube. They examined some IN molecules that can be easily encapsulated within the single-walled carbon nanotube cavity by molecular dynamics simulation [6]. In their research on the interaction of DNA and IN using various spectroscopic methods such as circular dichroism, fluorimetry, UV absorption, viscometric techniques, and competition analysis, they reported that IN can bind to circulating tumor DNA (CT-DNA) through groove binding [7].

Studies such as the interaction of alkali and alkali metal cations with benzene and substituted benzene derivatives have been conducted to understand fundamental aspects of the between π and cation interaction and the strength of these interactions [8, 9]. The role of cation-π interaction in substituted benzene and borazine with (Li^+, Na^+, and K^+) ions through DFT and ab initio quantum chemical studies at different theoretical levels has been elucidated [8].

✉ Fatma Genc
ftmgenc@yahoo.com

[1] Department of Analytical Chemistry, Faculty of Pharmacy, Istanbul YeniYuzyil University, Istanbul, Turkey

[2] Biomedical Engineering Department, Faculty of Engineering & Architecture, Kastamonu University, Kastamonu, Turkey

[3] Department of Physics, Atomic and Molecular Physics, Faculty of Science, Trakya University, Edirne, Turkey

Various alumaphosphinine ring complexes with alkali metal cations (K^+, Na^+, and Li^+) and alkaline earth metal cations such as Ca^{2+}, Mg^{2+}, and Be^{2+} at the B3LYP/6–311 + + G(d,p) level had been optimized and then performed single point calculations with MP2 functionals and 6–311 + + G(d,p) basis set to describe the aromaticity change for the alumaphosphinine ring induced upon complexation and reported that HOMA, PDI, and FLU decreased in aromaticity upon complexation [10].

The main purpose of this study is to define the type of interactions between main group metal cations and IN molecules. We know that no comparative research has been investigated before regarding the interactions of lithium, sodium, and potassium cations with the IN molecule. For this purpose, a comparative study of the change in different properties of electronic, structural, and sensing of free IN molecules and complexes has been obtained with the adsorption of lithium, sodium, and potassium cations to the IN molecule.

In this work, the topology analysis to define the interaction between IN and lithium, sodium, and potassium cations using QTAIM and non-covalent interactions (NCI) with reduced density gradient (NCI-RDG) has also been studied. The frontier molecular orbital (FMO) analysis of the studied complexes has been obtained by the density of states (DOS). HOMA analysis was performed to investigate the effects of these cations on the aromaticity of IN in the complexes obtained by interacting with lithium sodium and potassium cations.

Quantum chemical calculations performed with the Gaussian 09 program package will make it easier to understand the effect of lithium, sodium, and potassium cations on IN molecule properties of sensing and the metal cations nano-carriers on IN in drug release studies.

Materials and methods

Computational methods

All beginning complex structures are designed with lithium sodium and potassium cations in two ways. In one way, the cations were located on the normal lines of the phenyl group belonging to IN. In another, cations were located near the oxygen atom of carbonyl groups belonging to IN. Calculations for under-study compounds have been performed using the Gaussian 09 program [11]. All complexes, metal ions, and IN are fully optimized at the B3LYP/6-311G(d,p) level of theory.

The interaction, desorption, and adsorption energies for IN complexes with metal ions have also been computed. All interaction energies have been corrected for basis set superposition errors (BSSE) using the balancing method of Boys and Bernardi [12].

The adsorption energy (ΔE_{ads}), the adsorption enthalpy (ΔH_{ads}), and the adsorption free energy (ΔG_{ads}) are predicted as follows:

$$\Delta A_{\text{ads}} = A_{\text{complex}(M/IN)} - \left(A_{IN} + A_M\right) + A(BSSE)\text{A} = \text{E, H, G} \tag{1}$$

where $A_{\text{complex}(M/IN)}$, A_{IN}, and A_M are the total energy of the complex, the isolated energies of the IN, and the metal cation, respectively. BSSE is shown as *A(BSSE)* term corrections obtained by the counterpoise method-CP [12]. The adsorption energy ΔA_{ads} of the complexes is given by the following equations [13]:

$$A_{\text{int(complex)}} = A_{\text{complex}(M/IN)} - (A_{IN\text{incomplex}} + A_{M\text{incomplex}}) \tag{2}$$

Deformation energy, shown as A_{def}, can be defined as

$$A_{\text{def}} = A_{\text{def}-IN} + A_{\text{def}-M} \tag{3}$$

where $A_{\text{def}-M}$ is the deformed energy of the metal ions adsorbed, $A_{\text{def}-IN}$ is because of the energy applied to change the IN drug from its isolated configuration to the relaxed molecule in the complex.

Additionally, charge transfers between IN and lithium, potassium and sodium cations were performed. Electrostatic potential surfaces (ESP) were visualized with Gauss View in the Gaussian 09 program package.

To extract topological parameters and understand the nature of interactions, QTAIM analysis based on Bader theory [14] was performed with the MULTIWFN 3.7 program [15]. Properties at bond critical points (BCPs) in lithium, sodium, and potassium cation-IN interactions were calculated by QTAIM analysis.

Weak interactions were distinguished by performing NCI analysis [15] based on the RDG of quantum mechanical electron density through the Multiwfn 3.7 program. RDG distribution plots were obtained against the second-largest eigenvalue of the Hessian electron density matrix with the Multiwfn 3.7 program. Color maps of the scattering points and surfaces of RDG were drawn using the gnuplot 5.7 program [16] and the visual molecular dynamics (VMD) package [17], respectively. MO analysis with a total density of states (TDOS) was also performed using the Gaussian Sum program [18].

The aromaticity for the IN ring and its complexes are measured using HOMA and bird aromaticity index [19, 20] using Multiwfn-3.7 [15].

Results and discussion

In this study, the complexes obtained with the interaction of IN and lithium, sodium, and potassium cations are considered. First, the metal cations are placed near the oxygen atom belonging to the carbonyl group. The metal cations on the top of the IN and both structures have been optimized at B3LYP/6-311G(d,p) level. The structures, map and HOMO, and LUMO images of IN and its optimized complexes with lithium, potassium, and sodium cations in both forms are given in Fig. 1. As can be seen from Fig. 1 and Table 1, the contribution of O11, O10, N1, C4, C5, C3, C2, C9, C6, C8, and C7 atoms of IN to HOMO is as percentages of 2.33, 7.82, 24.31, 12.09, 12.83, 0.33, 0.98, 2.72, 10.28, 21.93, and 3.83. The contribution of O11, O10, N1, C4, and C6 atoms to HOMO decreases, and the contribution of C5, C3,C2, C9, C8, and C7 atoms to HOMO increases at $[Li\text{-}IN_a]^+$, $[Na\text{-}IN_a]^+$, and $[K\text{-}IN_a]^+$ complexes. The contribution of N1, C4, C5, C9, C6, C8, and C7 atoms to HOMO decreases, and the contribution of O11, O10, C3, and C2 atoms to HOMO increases

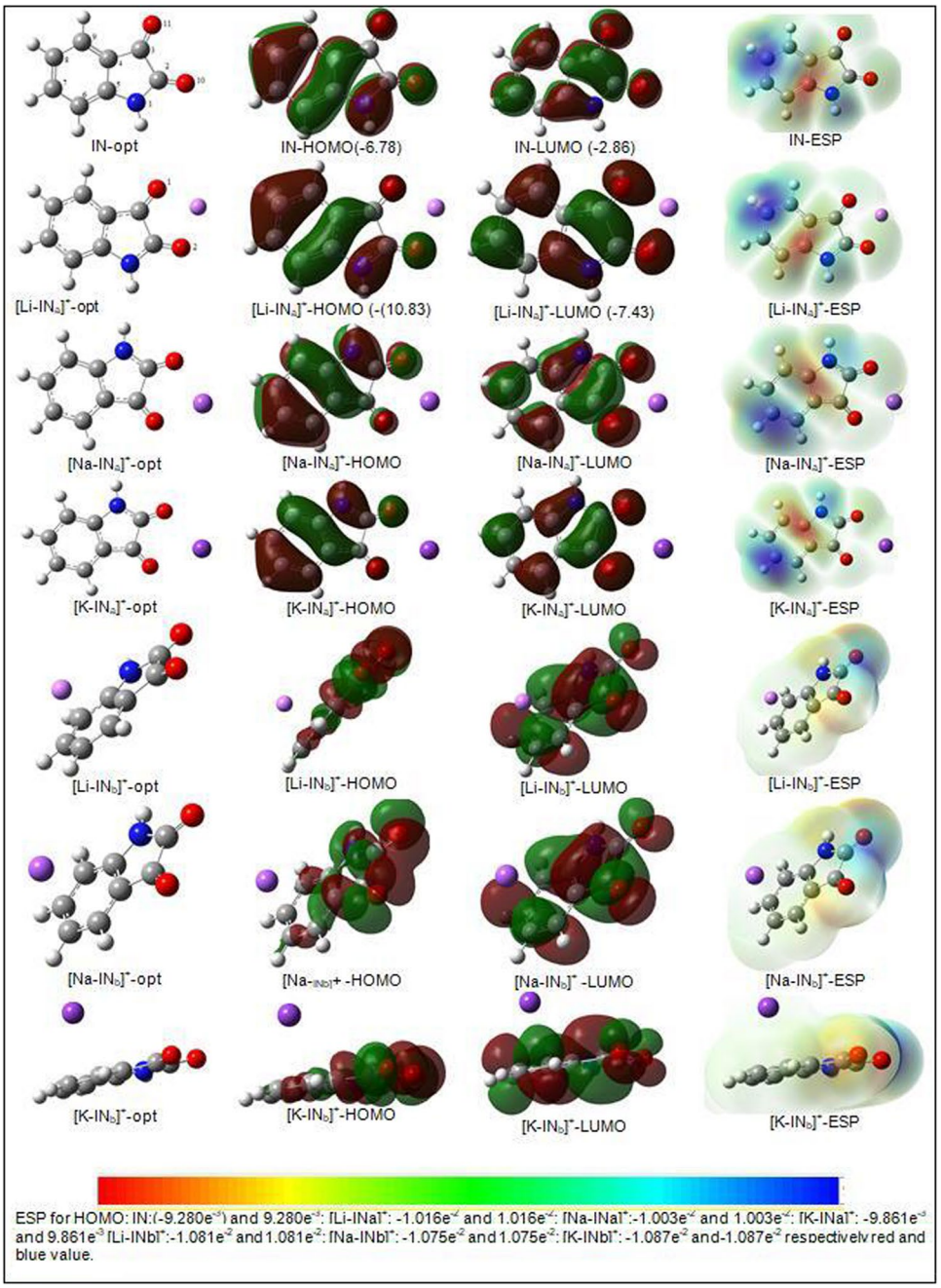

Fig. 1 The optimized structures, HOMO–LUMO map of the structures, and ESP surfaces

Table 1 Contribution of atoms to HOMO and LUMO

		O11	O10	N1	C4	C5	C3	C2	C9	C6	C8	C7
IN	HOMO	2.33	782	24.31	12.09	12.83	0.33	0.98	2.72	10.28	21.93	3.83
$[Li\text{-}IN_a]^+$		1.58	5.22	15.60	8.57	17.76	0.70	1.87	7.56	10.00	25.95	4.61
$[Li\text{-}IN_b]^+$		32.79	33.61	4.95	7.95	0.41	8.51	8.51	0.6	0.59	0.42	0.07
$[Na\text{-}IN_a]^+$		1.65	5.62	16.95	9.12	17.02	0.67	1.73	6.80	10.10	25.38	4.39
$[Na\text{-}IN_b]^+$		33.24	33.03	4.82	7.85	0.41	8.59	8.67	0.65	0.58	0.43	0.07
$[K\text{-}IN_a]^+$		1.73	5.92	17.91	9.56	16.53	0.63	1.63	6.17	10.09	24.97	4.32
$[K\text{-}IN_b]^+$		33.38	32.70	4.80	7.78	0.42	8.65	8.75	0.70	0.61	0.46	0.07
IN	LUMO	20.66	9.91	0.79	5.56	6.67	22.10	10.87	9.41	0.91	0.87	12.01
$[Li\text{-}IN_a]^+$		17.37	8.79	2.34	1.54	7.17	25.59	13.61	9.81	0.40	0.51	11.23
$[Li\text{-}IN_b]^+$		19.26	8.11	0.20	11.05	6.27	17.09	6.95	10.68	3.22	1.13	14.90
$[Na\text{-}IN_a]^+$		18.29	9.32	2.01	1.91	7.12	25.48	13.39	9.52	0.33	0.53	11.02
$[Na\text{-}IN_b]^+$		19.57	8.50	0.26	9.58	6.48	18.17	7.57	10.60	2.75	0.98	14.59
$[K\text{-}IN_a]^+$		18.92	9.59	1.81	2.28	7.07	25.18	13.19	9.36	0.31	0.55	10.91
$[K\text{-}IN_b]^+$		19.92	8.87	0.33	8.43	6.63	19.16	8.15	10.52	2.23	0.87	14.01

at $[Li\text{-}IN_a]^+$, $[Na\text{-}IN_a]^+$, and, $[K\text{-}IN_a]^+$ complexes. The LUMO orbital of IN is composed of mainly O11, O10, C4, C5, C3, C2, C9, and C7. In the contribution of these atoms to HOMO as percentages of 20.66, 9.91, 5.56, 6.67, 22.10, 10.87, 9.41, and 12.01 for IN, the contribution of C4 atom to LUMO decreases to 1.54 for $[Li\text{-}IN_a]^+$ complex and increases to 11.05 for $[Li\text{-}IN_a]^+$ complex. The color scale given below in Fig. 1 shows the change in HOMO charge densities of ESP graphs presented in the last column for the studied molecules from a negative charge value (red color) to a positive charge value (blue color). Green color codes also indicate that it is neutral.

For $[Li\text{-}IN_a]^+$, $[Na\text{-}IN_a]^+$, and $[K\text{-}IN_a]^+$ complexes, cation–O11 bonds are shorter compared to the metal–O10 bonds. It is seen that the distance of the ions to the oxygen atoms of IN increases with the increase of ion size from lithium cation to potassium cation, and also, the distance of the center of the phenyl group of IN increases with the increase of ion size from lithium cation to potassium cation. The binding energies of IN complexes are calculated in terms of gas phase electronic energy, enthalpy, and Gibbs free energy, as summarized in Table 2. The adsorption, interaction, and deformation energy for $[Li\text{-}IN_a]^+$ and $[Li\text{-}IN_b]^+$ were calculated with the wB97XD functional using a version of Grimme's D2 dispersion model [21] and were given in Table 2.

As predicted in Table 2, the adsorption energy, enthalpy, and Gibbs free energy of these complexes decrease with the increase of cation size from lithium to potassium. The interaction energy values decreased with the increase of the

Table 2 The adsorption energy, Gibbs free energy, and enthalpy in the gas phase for studied structures

		ΔE	ΔH	ΔG		ΔE	ΔH	ΔG
B3lyp/6-311G(d,p)								
$[Li\text{-}N_a]^+$	A_{ads}	−64.70	−65.59	−57.17	$[Li\text{-}N_b]^+$	−26.90	−27.53	−19.64
	A_{int}	−69.86	−70.60	−62.55		−37.97	−38.71	−30.72
	A_{def}	5.16	5.01	5.38		11.07	11.18	11.07
$[Na\text{-}N_a]^+$	A_{ads}	−48.82	−49.28	−41.22	$[Na\text{-}N_b]_+$	−14.68	−14.82	−7.83
	A_{int}	−51.52	−51.86	−44.11		−15.39	−15.54	−8.50
	A_{def}	2.71	2.59	2.89		0.71	0.73	0.67
$[K\text{-}IN_a]^+$	A_{ads}	−18.24	−17.71	−5.64	$[K\text{-}IN_b]^+$	−22.25	−22.09	−8.25
	A_{int}	−21.28	−20.81	−7.99		−24.23	−23.93	−9.84
	A_{def}	3.04	3.10	2.35		1.98	1.84	1.59
wB97XD/6-311G(d,p)								
$[Li\text{-}N_a]^+$	A_{ads}	−60.54	−61.35	−53.10	$[Li\text{-}IN_b]^+$	−26.59	−27.16	−19.43
	A_{int}	−65.32	−65.98	−58.09		−27.51	−28.10	−20.29
	A_{def}	4.78	4.63	4.99		0.92	0.94	0.87

SEZPE sum of electronic and zero-point energies, *SETEn* sum of electronic and thermal enthalpies, *SETFE* sum of electronic and thermal free energies

equilibrium distance of the cation from the oxygen atoms of the carbonyl group or the geometric center of the phenyl ring [10].

The adsorption energy values have the following order: $[Li\text{-}IN_a]^+ > [Na\text{-}IN_a]^+ > [K\text{-}IN_a]^+$ for the interaction oxygen atoms of IN with metal ions, and $[Li\text{-}IN_b]^+ > [Na\text{-}IN_b]^+ > [K\text{-}IN_b]^+$ for the interaction phenyl group of IN with metal ions. Deformation energy values for $[Li\text{-}IN_a]^+ > [Na\text{-}IN_a]^+ > [K\text{-}IN_a]^+$ are 5.16, 2.71, 3.04 kcal/mol and 11.07, 0.71, 1.98 kcal/mol. As seen, the adsorption energy values are found to be strongly dependent on the size of the cation in both calculations [8]. The ΔH and ΔG values for the B3LYP and wB97XD functionals were negative, confirming that the examined systems showed a spontaneous tendency [22].

Charge transfer (CT) and Mulliken atomic charges

The amount of CT between IN and a cation is easily determined as the difference between the isolated cation's charge and the metal's atomic charge in the corresponding complexes. The larger radius of the metal ion is, the less electron density can be transferred from the neutral IN to the metal ion for both interactions. So, the transferred charge between IN and metal cations during complexation can indicate the adsorption strength between the IN and the cations for both complexations. The charge transfers between IN and metal cations during the interaction are given in Table 3.

In Table 3, the smallest charge transfer belongs to the IN-K^+ complexes. This means less charge on Li^+ cation with respect to other metal cations in the complexes. So, most of the charge transfers and interaction energy values are seen in $[Li\text{-}IN_a]^+$ complex, while the least one is seen in $[K\text{-}IN_b]^+$ complex (Table 3).

Topology analysis

Quantum theory of atoms in molecules

To learn more about bonding for IN with M (Li^+, Na^+, and K^+ ion), topological analysis was performed and corresponding wave functions were generated at the same theory level. The properties in terms of electron density ($\rho(\boldsymbol{r})$) and Laplacian ($\nabla^2\rho(\mathbf{r})$), total electron energy density ($V(\boldsymbol{r})$), potential electron energy density ($V(\boldsymbol{r})$), and Lagrange kinetic energy ($G(\mathbf{r})$) at the intramolecular BCPs were obtained (Table 4). The observed molecular topological map of C = O groups and phenyl group of IN with Li^+ Na^+ and K^+ ion is provided in Fig. 2.

AIM theory [23] states that the existence of an interaction corresponds to the existence of a bond path between the donor and acceptor, which includes the BCP in the topological analysis of the electron density distribution. In general, $\rho(\mathbf{r})$ is greater than 0.20 a.u in shared (covalent) bonding and less than 0.10 a.u in a closed-shell interaction (for example, ionic, van der Waals, hydrogen, dihydrogen, and H–H bonding) [24].

The Laplacian of $\rho(\boldsymbol{r})$ being related to the bond interaction energy is expressed as follows by viral theorem:

Table 3 Charge transfer values are deduced from Mulliken atomic charges during the interaction between IN and metal cations

Complex	O11-Li	O10-Li	CT(IN_a-M)	Complex	Phen-Li	CT(IN_a-M)
$[Li\text{-}IN_a]^+$	1.96665	1.93411	0.690664	$[Li\text{-}IN_a]^+$	1.89907	0.383667
$[Na\text{-}N_a]^+$	2.32724	2.30015	0.212513	$[Na\text{-}N_b]^+$	2.48076	0.17889
$[K\text{-}IN_a]^+$	2.70279	2.65622	0.127519	$[K\text{-}IN_b]^+$	2.97839	0.090571

Table 4 Kinetic energy density (G), the electron density (ρ), total electron energy density (H), potential energy density (V), and Laplacian of electron density ($\nabla^2\rho$) at BCPs in the IN-adsorbed compounds by QTAIM analysis

Struc	Atoms	ρ_{BCP}	G_{BCP}	V_{BCP}	H_{BCP}	$\nabla^2\rho_{BCP}$	$\lvert V_{BCP}\rvert / G_{BCP}$
$[Li\text{-}IN_a]^+$	O11-Li	0.02792307980	0.03890655863	-0.03110269627	0.007803862362	0.1868416840	0.7994204
	O10-Li	0.03021731125	0.04326507298	-0.03449413753	0.008770935450	0.2081440337	0.7972745
$[Li\text{-}IN_{ab}]^+$	Phen-Li	0.01888603202	0.02128993928	-0.01803727365	0.003252665623	0.0981704196	0.8472205
$[Na\text{-}IN_a]^+$	O11-Na	0.02132646786	0.02654545088	-0.02144464236	0.005100808521	0.1265850376	0.8078462
	O10-Na	0.02263229454	0.02880287079	-0.02320498336	0.005597887424	0.1376030328	0.8056483
$[Na\text{-}IN_b]^+$	Phen-Na	0.01221008733	0.01162476990	-0.009307484342	0.002317285558	0.0557682218	0.8006597
$[K\text{-}IN_a]^+$	O11-K	0.01836135905	0.01716300504	-0.01448460562	0.002678399425	0.0793656178	0.8439434
	O10-K	0.02020860376	0.01943847773	-0.01642569722	0.003012780510	0.0898050329	0.8450094
$[K\text{-}IN_b]^+$	Phen-K	0.00933858543	0.00691973535	-0.00531069187	0.001609043473	0.0341151153	0.7674704

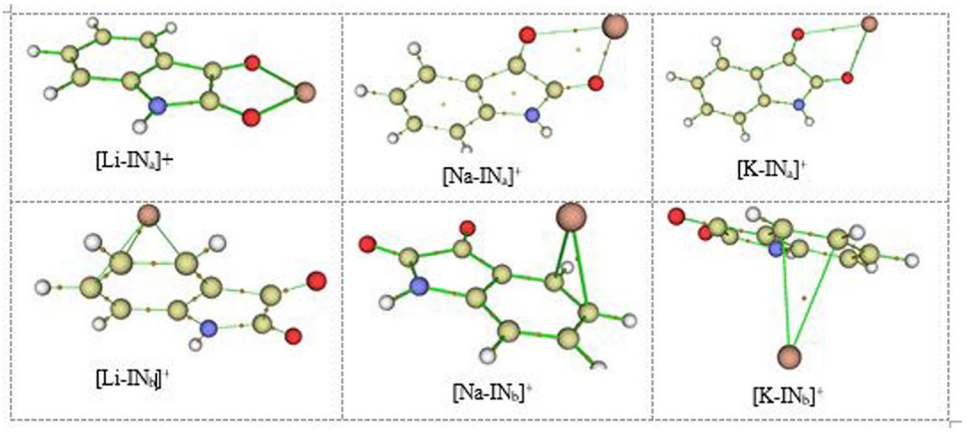

Fig. 2 The molecular topological maps of IN-metal cation complexes

$$\frac{1}{2}\nabla^2\rho(\mathbf{r}) = 2G(\mathbf{r}) + V(\boldsymbol{r}) \tag{4}$$

where $\nabla^2\rho(\mathbf{r})$, $V(\boldsymbol{r})$, and $G(\mathbf{r})$ denote the excess potential energy, the electronic potential energy density, and the electronic kinetic energy density at BCP.

A positive $\nabla^2\rho(\mathbf{r})$ in a BCP indicates that the contribution of kinetic energy is greater than potential energy, and a positive $\nabla^2\rho(\mathbf{r})$ in a BCP indicates that the electronic charge is depleted along the bond path. Charge concentration occurs in the bonding region when $\nabla^2\rho(\mathbf{r}) < 0$, and the charge depletion occurs when If $\nabla^2\rho(\mathbf{r}) > 0$.

In contrast, in closed-shell bonding, van der Waals interactions, and ionic hydrogen bonding, the interaction is characterized by a decrease in density in the interacting region of the two atoms. In covalent bonding, the two negative curvatures are dominant and $\nabla^2\rho(\mathbf{r}) < 0$ [24].

When $\frac{V(\boldsymbol{r})}{G(\mathbf{r})} > 1$, the charge reduction can also lead to a local accumulation of charge, resulting in a relatively stable bond dominated by potential energy. When the viral energy theorem is coupled with force, $H(\mathbf{r}) < 0$ and $(\mathbf{r}) > 0$ strongly indicate stable bonding and pure closed-shell interaction, respectively. $H(\mathbf{r})$ can be calculated as follows:

$$H(\mathrm{r}) = G(\mathrm{r}) + V(r) \tag{5}$$

[Li-IN$_a$]$^+$, [Na-IN$_a$]$^+$, and [K-IN$_a$]$^+$ configurations in gas phase positive values of $\nabla^2\rho(\mathbf{r})$(0.1868416840, 0.1265850376, and 0.0793656178 for C = O11 group of IN and M ion interaction and 0.2081440337 a.u., 0.1376030328 a.u., and 0.0898050329 a.u. for C = O10 and M ion interaction) and H (0.001 a.u.) and [Li-IN$_b$]$^+$, [Na-IN$_b$]$^+$, and [K-IN$_b$]$^+$ configurations in gas phase positive values of $\nabla^2\rho(\mathbf{r})$(0.0981704196, 0.0557682218, and 0.0341151153 for phenyl group of IN and M ion interaction and 0.2081440337 a.u., 0.1376030328 a.u., and 0.0898050329 a.u. for C = O10 and M ion interaction) indicate a depletion of density in the region of contact of the two atoms and are characterized by ionic interaction.

At BCPs, the computed values of ρ_c of the [Li-IN$_a$]$^+$, [Na-IN$_a$]$^+$, and [K-IN$_a$]$^+$ configurations in gas phase 0.02792307980, 0.02132646786, and 0.01836135905 for C = O11 and M ion interaction, respectively, and 0.03021731125, 0.02263229454, and 0.02020860376 for C = O10 and M ion interaction.

Non-covalent interactions (NCI) analysis-reduced density gradient (RDG)

NCI analysis is the second most powerful way to visualize the types of intermolecular interactions based on the average RDG function defined in the figure below.

$$RDG(\boldsymbol{r}) = \frac{1}{2(3\pi^2)^{1/3}} \frac{|\Delta\rho(\mathbf{r})|}{\rho(\boldsymbol{r})^{4/3}} \tag{6}$$

NCI index, defined by Johnson et al., is used to investigate the presence of weak [25]. The $\rho(\boldsymbol{r})$ values represent the strength of bonds and the function with sign λ2, where λ2 is referred to as the second-largest eigenvalue of the Hessian matrix of $\rho(\boldsymbol{r})$. The nature and strength of the interaction are assessed by the NCI chart. Therefore, NCI plots are created to investigate the presence of weak interactions. For each specific value of RDG, as shown in a horizontal line on the NCI plots, the regions of the plots can be shown as red, green, and blue color codes corresponding to the repulsion, Wander-Waals forces, and strong electrostatic interactions, respectively. The interactions are repulsive if (sign λ2) $\rho(\boldsymbol{r})$ >0, attractive if (sign λ2) $\rho(\boldsymbol{r})$<0, and van der Waals type if (sign λ2) $\rho(\boldsymbol{r}) \leq 0$. The RDG scatter plots versus (sign λ2) ρ(r) of some selected complexes are illustrated on the left side of Fig. 3. [Li-IN$_a$]$^+$ and [K-IN$_b$]$^+$ complexes are preferred due to having the most and the minor charge transfers and interaction energy values in Table 3, respectively. The color code diagram for the RDG scatter plots based on the type of interaction is given at the top of Fig. 3. Color-mapped RDG isosurface graphs deduced from Multiwfn and

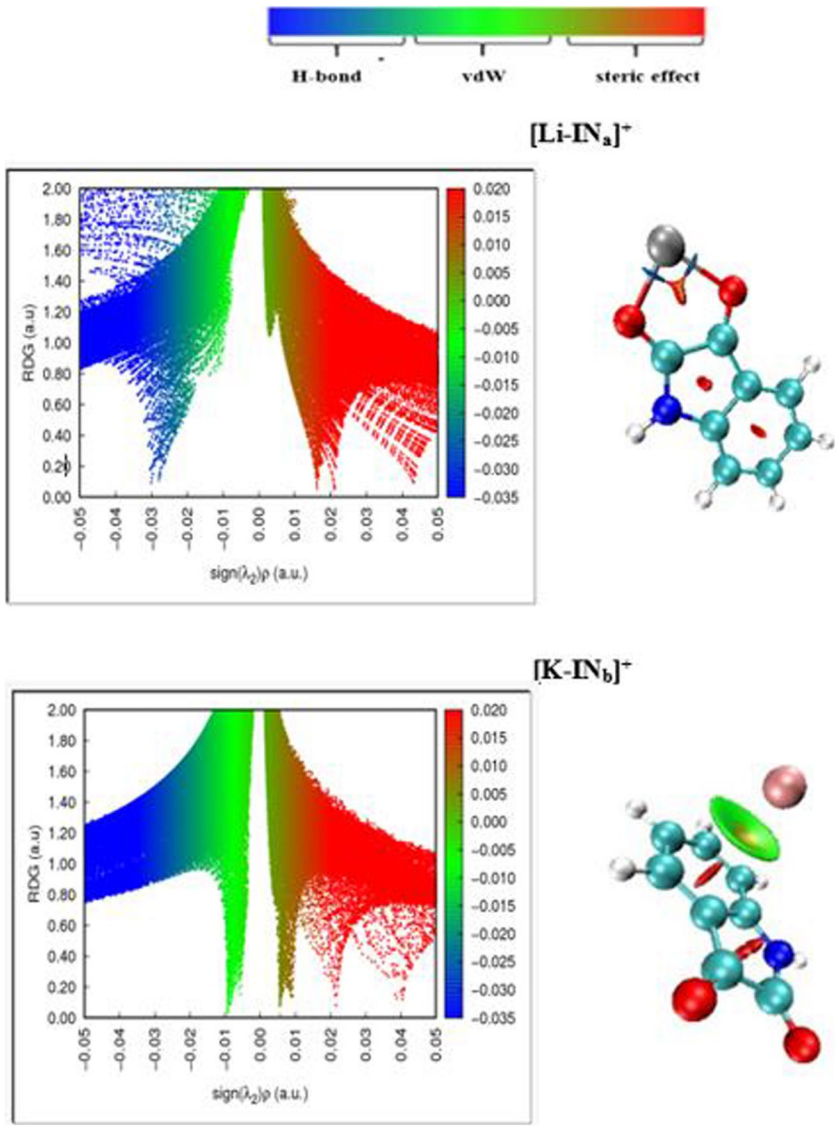

Fig. 3 The RDG scatter plots (left) and the color-filled RDG isosurfaces (right) for (**a**) [Li-IN$_a$]$^+$ and (**b**) [K-IN$_b$]$^+$ complexes

VMD programs are also shown on the right-hand side of Fig. 3. The red- and blue-filled circles in the RDG isosurface graphs correspond to the repulsive and attractive interactions between atoms. Color codes such as green–brown or green circles indicate van der Waals interactions (Fig. 3).

In Fig. 3a, the two spikes in the blue region according to the value of (sign λ2) ρ(r) ranging from − 0.028 to − 0.05 a.u are used to describe the partially ionic interactions between Li-ion and IN molecule. The three spikes in the red region ranging from 0.015 to 0.05 a.u to the value of (sign λ2) ρ(r) in the RDG scatter plots of [Li-IN$_a$]$^+$ describe the stabilizing steric interactions due to the red-filled circles of the rings in color RDG isosurface at the right-hand side in Fig. 3 (upper case). On the right-hand side in Fig. 3a, the blue color-filled circles on the bonds between Li-ion and oxygen atoms of the IN molecule show the RDG isosurfaces, indicating the existence of attractive interactions.

In Fig. 3 (lower case), the four red spikes at (sign λ2) ρ(r) value in the 0.005 to 0.04 regions indicate the destabilizing interactions for the [K-IN$_b$]$^+$ complex. The red circles are observed in the center of rings of the IN molecule illustrated on the right-hand side of Fig. 3 showing a strong steric effect.

There is a weak vdW-type interaction due to the spike placed in the green region at − 0.01 a.u of (sign λ2) ρ(r) for the [K-IN$_b$]$^+$. The big green-yellow color circle between the K ion and IN molecule at the color-filled RDG isosurfaces is in Fig. 3. These colored RDG isosurfaces and spikes indicate the existence of non-covalent interaction between alkali metal ions and IN molecules.

Frontier molecular orbital (FMO) analysis

FMO analysis is based on the HOMO and LUMO energies and the HOMO–LUMO energy gap, which is the difference between HOMO energy and LUMO energy of the IN and its complexes with the lithium, potassium, and sodium cations before and after interaction has been utilized and illustrated in Fig. 4. E_{HOMO} and E_{LUMO} were computed at the B3LYP level with 6–311 + G(d) basis set and were given in Fig. 4.

In Fig. 4, E_{HOMO} and E_{LUMO} decrease remarkably after IN adsorption to lithium, potassium, and sodium cations. The HOMO energy of IN is – 6.78 eV, while that of $[Li\text{-}IN_a]^+$, $[Li\text{-}IN_b]^+$, $[Na\text{-}IN_a]^+$, $[Na\text{-}IN_b]^+$, $[K\text{-}IN_a]^+$, and $[K\text{-}IN_b]^+$ complexes is – 10.83 eV, – 11.02 eV, – 10.41 e V, – 10.59 eV, – 10.08 eV, and – 10.32 eV. The most significant energy reduction in HOMO was observed in the $[Li\text{-}IN_b]^+$ complex. The LUMO energy of IN is – 2.86 eV, and the greatest energy reduction for LUMO was observed in the $[Li\text{-}IN_b]^+$ complex.

E_{HOMO}, E_{LUMO}, and band gap (Eg) provide information about the decrease or increase in chemical stability and chemical reactivity of a system. As the energy gap (Eg) increases, chemical reactivity decreases. The energy gap of IN is 3.92 eV, those of $[Li\text{-}INa]^+$, $[Na\text{-}INa]^+$, and $[K\text{-}INa]^+$ complexes are 3.40 eV, 3.71 eV, and 3.47 eV, and those of $[Li\text{-}INb]^+$, $[Na\text{-}INb]^+$, and $[K\text{-}INb]^+$ complexes are 3.77 eV, 3.53 eV, and 3.82 eV, which indicate that if metal ion interacts with the phenyl group of the IN, HOMO–LUMO energy gap is more affected.

The DOS plot of Isatin is given in Fig. 5 by comparison with the DOS graph of $[Li\text{-}INa]^+$ complex, which shows the metal cation complex with the lowest energy gap.

The most percentage change in Eg as %ΔEg is a decrease of 13.265% calculated for the $[Li\text{-}INa]^+$ complex. It agrees with the charge transfer values given in Table 3. The lower the ΔEg, the better the electron transfer process can be. The most charge transfer value in Table 3 has been calculated for the $[Li\text{-}INa]^+$ complex.

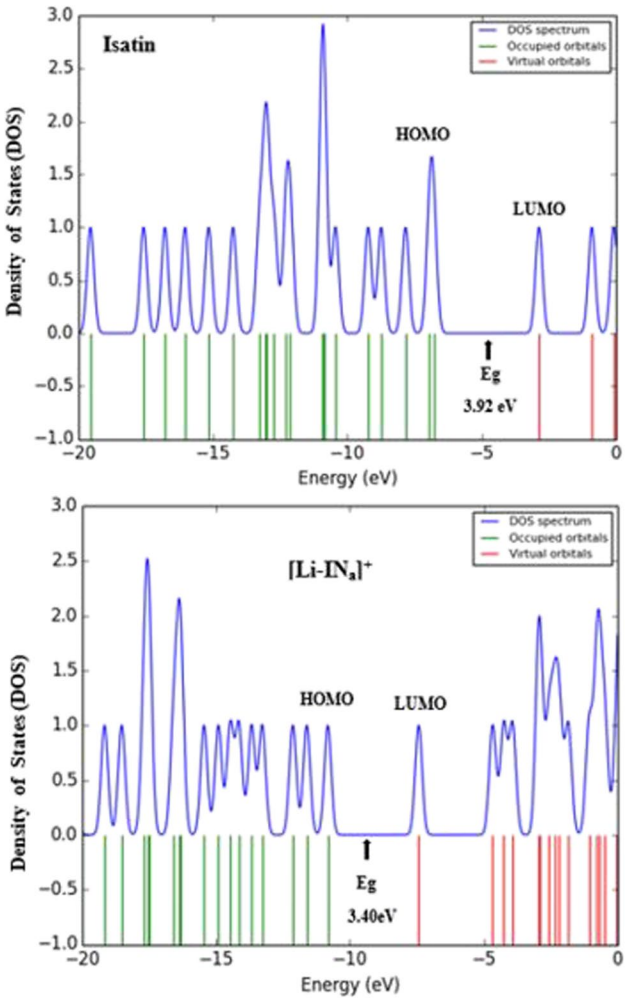

Fig. 5 The DOS graphs for (**a**) Isatin and (**b**) $[Li\text{-}INa]^+$ complex

HOMA and BIRD aromaticity index analysis

The harmonic oscillator aromaticity measurement (HOMA) index is known as displacement in cyclic structures and was defined by Kruszewski and Krygowski [26–28]. It is one of the most popular indexes for measuring aromaticity.

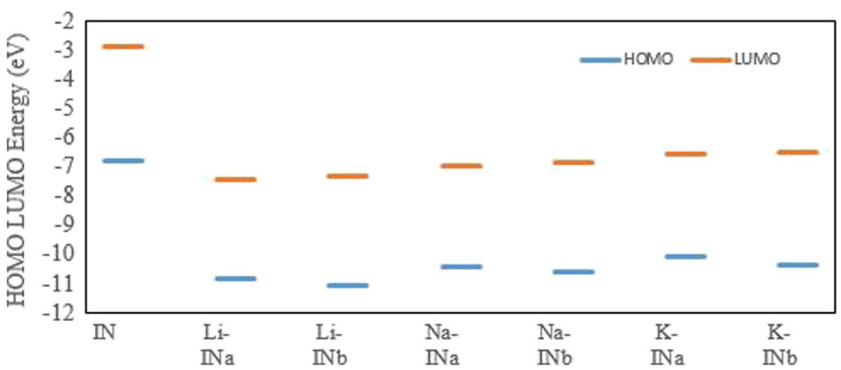

Fig. 4 E_{HOMO} and E_{LUMO} for the IN and complexes of IN with lithium, potassium, and sodium cations

Table 5 The HOMA and BIRD aromaticity index for IN-metal cation complexes

	IN	$[Li\text{-}IN_a]^+$	$[Li\text{-}IN_b]^+$	$[Na\text{-}IN_a]^+$	$[Na\text{-}IN_b]^+$	$[K\text{-}IN_a]^+$	$[K\text{-}IN_b]^+$
Bonds	Atom pair contribution to HOMA index						
C9-C4	−0.000049	−0.00455	−0.001107	−0.003364	−0.000880	−0.002555	−0.000617
C4-C5	−0.015338	−0.03398	−0.040319	−0.026195	−0.031829	−0.023128	−0.026408
C5-C9	−0.000063	−0.00670	−0.009537	−0.004401	−0.004994	−0.003306	−0.002676
C6-C7	−0.005141	−0.01349	−0.012114	−0.010793	−0.009236	−0.009281	−0.007076
C7-C8	−0.003953	−0.00437	−0.015130	−0.004558	−0.013691	−0.004471	−0.010579
C8-C9	−0.001640	−0.00033	−0.012312	−0.000371	−0.009317	−0.000490	−0.005650
HOMA	0.973816	0.936574	0.909479	0.950318	0.930053	0.956769	0.946992
Bonds	Atom pair contribution to BIRD aromaticity index						
C9-C4	1.814235	1.767846	1.793957	1.775054	1.796728	1.780736	1.800432
C4-C5	1.725453	1.680807	1.668821	1.697309	1.685152	1.704510	1.696824
C5-C6	1.825814	1.884009	1.745052	1.871689	1.765429	1.864685	1.779830
C6-C7	1.764645	1.731192	1.735746	1.740372	1.746219	1.746046	1.755252
C7-C8	1.771346	1.768908	1.726080	1.767821	1.730556	1.768310	1.741149
C8-C9	1.788416	1.805509	1.735076	1.804734	1.745905	1.802521	1.762017
BIRD	94.388074	89.329833	93.644906	90.838593	94.152504	91.631406	94.441066

The HOMA index estimates an aromatic character of the π-electron systems (molecules, ions, or their fragments) built up by the following bonds: CC, CN, CO, CP, CS, NN, and NO. BIRD index can describe the geometry-based aromaticity of the studied compounds. These indices are one of the best methods to describe the change in aromaticity [29]. Here, both indices were calculated by the MULTIWFN program and given in Table 5 for the studied complexes.

If HOMA is one [30], the compound is fully aromatic; if HOMA is zero (0), the compound or ring is not fully aromatic. The HOMA values of IN, $[Li\text{-}INa]^+$, $[Na\text{-}INa]^+$, and $[K\text{-}INa]^+$ are 0.973816, 0.936574, 0.950318, and 0.956769.

Relative aromaticity trends among the computed compounds are thus IN > $[K\text{-}IN_a]^+$ > $[Na\text{-}IN_a]^+$ > $[K\text{-}IN_b]^+$ > $[Li\text{-}INa]^+$ > $[Na\text{-}IN_b]^+$ > $[Li\text{-}IN_b]^+$, which denotes aromaticity is affected by the interaction of IN and metal cation.

Conclusions

IN, $[Li\text{-}IN_a]^+$, $[Na\text{-}IN_a]^+$, $[K\text{-}IN_a]^+$, $[Li\text{-}IN_b]^+$, $[Na\text{-}INb]^+$, and $[K\text{-}IN_b]^+$ were calculated theoretically in the gas media with the DFTB3LYP/6-311G(d,p) level of theory. The HOMA index for the phenyl ring of IN was 0.973816, and the HOMA value with the interaction of IN and metal cation decreased. HOMO–LUMO energy difference for IN, $[Li\text{-}IN_a]^+$, $[Na\text{-}IN_a]^+$, $[K\text{-}IN_a]^+$, $[Li\text{-}IN_b]^+$, $[Na\text{-}INb]^+$, and $[K\text{-}IN_b]^+$ was found as 6.04 eV.

Surface maps of the IN, $[Li\text{-}IN_a]^+$, $[Na\text{-}IN_a]^+$, $[K\text{-}IN_a]^+$, $[Li\text{-}IN_b]^+$, $[Na\text{-}INb]^+$, and $[K\text{-}IN_b]^+$ complexes were drawn with GaussView5. The map visualizes the charge regions of the molecule, with red and blue colors on the scale bar indicating negative and positive parts, respectively. Based on the QTAIM results, the IN interactions with metal cations are the non-covalent character. It was observed in the RDG scatter plots a weak vdW-type interaction order due to the spike placed in the green region based on the values of (sign λ2) ρ(r) as for the $[Li\text{-}IN_b]^+$ > $[Na\text{-}IN_b]^+$ > $[K\text{-}IN_b]^+$. This is also evidenced by the color-filled RDG isosurfaces created with VMD for $[Li\text{-}IN_b]^+$ and $[K\text{-}IN_b]^+$ complexes. The difference between the charge distribution of the IN molecule and the charge distribution of the complexes can be seen from the MEP map. According to the HOMA and BIRD aromaticity index, the aromaticity order was found as IN > $[K\text{-}IN_a]^+$ > $[Na\text{-}IN_a]^+$ > $[K\text{-}IN_b]^+$ > $[Li\text{-}IN_a]^+$ > $[Na\text{-}IN_b]^+$ > $[Li\text{-}IN_b]^+$. The ΔH and ΔG values were negative, confirming that the examined systems showed a spontaneous tendency.

Author contributions All authors contributed to the study conception and design. Material preparation, data collection and analysis were performed by FK and SŞD. The first draft of the manuscript was written by FK, SŞD and FG and all authors commented on previous versions of the manuscript. All authors read and approved the final manuscript. All authors reviewed the manuscript.

Data availability The datasets generated during and/or analyzed during the current study are available from the corresponding author upon reasonable request.

Declarations

Competing interests The authors declare no competing interests.

References

1. Pandeya SN, Smitha S, Jyoti M, Sridhar SK (2005) Biological activities of isatin and its derivatives. Acta Pharm 55(1):27–46
2. Pakravan P, Kashanian S, Khodaie MM, Harding FJ (2013) Biochemical and pharmacological characterization of isatin and its derivatives: from structure to activity. Pharmacol Rep 65(2):313–335. https://doi.org/10.1016/S1734-1140(13)71007-7
3. Halket JM, Watkins PJ, Przyborowska A, Goodwin BL, Clow A, Glower V, Sandler MJ (1991) Isatin (indole-2,3-dione) in urine and tissues. Detection and determination by gas chromatography-mass spectrometry. Journal of Chromatograpy 562:279–287. https://doi.org/10.1016/0378-4347(91)80585-Z
4. Silva JFM, Garden SJ, Pinto AC (2001) The chemistry of isatins: a review from 1975 to 1999. J Braz Chem Soc 12(3):273–324. https://doi.org/10.1590/S0103-50532001000300002
5. Matos MAR, Miranda MS, Morais VMF, Liebman JF (2003) Are isatin and isatoic anhydride antiaromatic and aromatic respectively? A combined experimental and theoretical investigation. Org Biomol Chem 1(14):2566–2571. https://doi.org/10.1039/B304405J
6. Dehaghani MZ, Yousefi F, Seidi F, Bagheri B, Mashhadzadeh AH, Naderi G, Esmaeili A, Abida O, Habibzadeh S, Saeb MR, Rybachuk M (2021) Encapsulation of an anticancer drug Isatin inside a host nano-vehicle SWCNT: a molecular dynamics simulation. Sci Rep 11:18753. https://doi.org/10.1038/s41598-021-98222-2
7. Kashanian S, Khodaei MM, Pakravan P (2010) Spectroscopic studies on the ınteraction of ısatin with calf thymus DNA. DNA Cell Biol 29(10):639–646. https://doi.org/10.1089/dna.2010.1054
8. Bania KK, Guha AK, Bhattacharyya PK, Sinha S (2014) Effect of substituent and solvent on cation–π interactions in benzene and borazine: a computational study. Dalton Trans 43(4):1769–1784. https://doi.org/10.1039/C3DT52081A
9. Dinadayalane TC, Afanasiev D, Leszczynski J (2008) Structures and energetics of the cation−π ınteractions of Li^+, Na^+, and $K^+$with cup-shaped molecules: effect of ring addition to benzene and cavity selectivity. J Phys Chem A 112(34):7916–7924. https://doi.org/10.1021/jp802236k
10. Ghenaatian HR (2017) Structural and electronic properties of alumaphosphinine complexes with metal ions: a theoretical study. Sci Iran Trans C: Chem Chem Eng 24(3):1181–1188. https://doi.org/10.24200/sci.2017.4099
11. Frisch MJ, Trucks GW, Schlegel HB, Scuseria GE, Robb MA, Cheeseman JR, Scalmani G, Barone V, Mennucci B, Petersson GA, Nakatsuji H, Caricato M, Li X, Hratchian HP, Izmaylov AF, Bloino J, Zheng G, Sonnenberg JL, Hada M, Ehara M, Toyota K, Fukuda R, Hasegawa J, Ishida M, Nakajima T, Honda Y, Kitao O, Nakai H, Vreven T, Montgomery JA Jr, Peralta JE, Ogliaro F, Bearpark M, Heyd JJ, Brothers E, Kudin KN, Staroverov VN, Kobayashi R, Normand J, Raghavachari K, Rendell A, Burant JC, Iyengar SS, Tomasi J, Cossi M, Rega N, Millam JM, Klene M, Knox JE, Cross JB, Bakken V, Adamo C, Jaramillo J, Gomperts R, Stratmann RE, Yazyev O, Austin AJ, Cammi R, Pomelli C, Ochterski JW, Martin RL, Morokuma K, Zakrzewski VG, Voth GA, Salvador P, Dannenberg JJ, Dapprich S, Daniels AD, Farkas Ö, Foresman JB, Ortiz JV, Cioslowski J, Fox DJ (2013) Gaussian 09. Gaussian Inc., Wallingford. https://doi.org/10.1017/CBO9781107415324.004
12. Boys SF, Bernardi R (1970) The calculation of small molecular interactions by the differences of separate total energies. Some procedures with reduced errors. Mol Phys 19(4):553–566. https://doi.org/10.1080/00268977000101561
13. DalgicSenturk S, Al-Sawaff ZH, Dalgic S, Kandemirli F (2023) A comparative DFT study on Al- and Si-doped single-wall carbon nanotubes (SWCNTs) for Ribavirin drug sensing and detection. Mater Sci Semicond Process 158:107360. https://doi.org/10.1016/j.mssp.2023.107360
14. Bader RFW (1985) Atoms in molecules. Acc Chem Res 18(1):9–15. https://doi.org/10.1021/ar00109a003
15. Lu T, Chen F (2012) Multiwfn: a multifunctional wave function analyzer. J Comput Chem 33(5):580–592. https://doi.org/10.1002/jcc.22885
16. Thomas W, Kelley C (2011) Gnuplot 4.5: an interactive plotting program. http://gnuplot.info. Accessed Oct 2023
17. Humphrey W, Dalke A, Schulten K (1996) VMD:visual molecular dynamics. J Mol Graphics 14(1):33–38. https://doi.org/10.1016/0263-7855(96)00018-5
18. O'Boyle NM, Tenderholt AL, Langner KM (2008) cclib: a library for package-independent computational chemistry algorithms. J Comput Chem 29(5):839–845. https://doi.org/10.1002/jcc.20823
19. Krygowski TM, Cyranski M (1996) Separation of the energetic and geometric contributions to the aromaticity. Part IV. A general model for the the (-electron systems. Tetrahedron 52(30):10255–10264. https://doi.org/10.1016/0040-4020(96)00560-1
20. Andrzejak M, Kubisiak P, Zborowski KK (2013) Avoiding pitfalls of a theoretical approach: the harmonicoscillator measure of aromaticity index from quantum chemistry calculations. Struct Chem 24:1171–1184. https://doi.org/10.1007/s11224-012-0148-2
21. Chai JD, Head-Gordon M (2008) Long-range corrected hybrid density functionals with damped atom–atom dispersion corrections. Phys Chem Phys 10:6615–6620. https://doi.org/10.1039/b810189b
22. de Miranda DB, Quintal S, Ferreira GB (2023) Theoretical studies of Zn^{2+} complexes with alkyl xanthate ligands: a thermochemical, electronic energy decomposition, and natural bond orbital analysis. J Mol Model 29:203. https://doi.org/10.1007/s00894-023-05604-
23. Bader RFW (1998) A bond path: A universal indicator of bonded interactions. J Phys Chem A 102:7314–7323. https://doi.org/10.1021/jp981794v
24. Matta CF, Boyd RJ (2007) In: the quantum theory of atoms in molecules: from solid state to DNA and drug design. An introduction to the quantum theory of atoms in molecules, 1st edn. https://doi.org/10.1002/9783527610709.ch1.
25. Johnson ER, Keinan S, Mori-Sánchez P, Contreras-García J, Cohen AJ, Yang W (2010) Revealing noncovalent interactions. J Am Chem Soc 132(18):6498–6506. https://doi.org/10.1021/ja100936w
26. Kruszewski J, Krygowski TM (1972) Definition of aromaticity basing on the harmonic oscillator model. Tetrahedron Lett 13(36):3839–3842. https://doi.org/10.1016/S0040-4039(01)94175-9
27. Krygowski TM (1993) Crystallographic studies of inter- and intramolecular interactions reflected in aromatic character of π-electron systems. J Chem Inf Comput Sci 33(1):70–78. https://doi.org/10.1021/ci00011a011
28. Krygowski TM, Cyrański M (1996) Separation of the energetic and geometric contributions to the aromaticity of π-electron carbocyclics. Tetrahedron 52(5):1713–1722. https://doi.org/10.1016/0040-4020(95)01007-6
29. Stanger A (2019) Reexamination of NICSπ, zz: height dependence, off-center values, and ıntegration. J Phys Chem A 123:3922–3927. https://doi.org/10.1021/acs.jpca.9b02083

30. Szymanski S, Majerz I (2019) Aromaticity and electron density of hypericin. J Nat Prod 82(8):2106–2115. https://doi.org/10.1021/acs.jnatprod.8b00872